J. Synchrotron Rad. (2000). **7**, 103–109

A conical slit for three-dimensional XRD mapping

S. F. Nielsen,[a]* A. Wolf,[b] H. F. Poulsen,[a] M. Ohler,[c] U. Lienert[a,c] and R. A. Owen[d]

[a]Materials Research Department, Risø National Laboratory, DK-4000 Roskilde, Denmark, [b]Institut für Mikrotechnik Mainz (IMM), Mainz, Germany, [c]European Synchrotron Radiation Facility, BP 220, F-38043, Grenoble, France, and [d]Manchester Materials Science Centre, University of Manchester and UMIST, Manchester M1 7HS, UK.
E-mail: soeren.faester.nielsen@risoe.dk

(*Received 8 September 1999; accepted 11 January 2000*)

Traditionally, depth resolution in diffraction experiments is obtained by inserting pinholes in both the incoming and diffracted beam. For materials science investigations of local strain and texture properties this leads to very slow data-acquisition rates, especially when characterization is performed on the level of the individual grains. To circumvent this problem a conical slit has been manufactured by wire-electrodischarge machining. The conical slit has six 25 μm-thick conically shaped openings matching six of the Debye–Scherrer cones from a face-centred-cubic powder. By combining the slit with a microfocused incoming beam of hard X-rays, an embedded gauge volume is defined. Using a two-dimensional detector, fast and complete information can be obtained regarding the texture and strain properties of the material within this particular gauge volume. The average machining and assemblage errors of the conical slit are found both to be of the order of 5 μm. An algorithm for alignment of the slit is established, and the potential of the technique is illustrated with an example of grain mapping in a 4.5 mm-thick Cu sample.

Keywords: X-ray powder diffraction; conical slits; texture; stress; strain; electrodischarge machining.

1. Introduction

Three-dimensional structural characterization is of much interest to materials science, as surface properties often are not representative of bulk behaviour. Most notably, *in situ* experiments related to annealing and deformation processes in general cannot be investigated by surface-sensitive techniques. At times there is also a need for studying embedded structures or truly three-dimensional properties such as stress fields non-destructively.

Until recently, bulk studies could only be performed by means of neutron diffraction, which has a limited spatial resolution, of the order of 1 mm^3. A synchrotron technique, based on microfocusing of hard X-rays, is now available with gauge volumes in the micrometre range and penetration power in the millimetre or centimetre range (Poulsen *et al.*, 1997; Lienert *et al.*, 1998). A dedicated instrument, a so-called 3DXRD microscope, has recently been commissioned at the materials science beamline of the ESRF (Lienert, Poulsen & Kvick, 1999). The instrument allows, for the first time, *in situ* investigations of such fundamental structures as the individual grains, inclusions or the surroundings of cracks. To fully exploit the potential of the hard X-rays, however, it is necessary to consider not only the spatial resolution but also the speed of the experimental procedure. This is especially true for materials science and engineering applications, which in general involve studying many points and many crystallographic orientations in the same sample as well as many samples and/or parameter settings.

Depth resolution in diffraction experiments is traditionally provided by a cross-beam technique with insertion of pinholes in both the incoming and diffracted beam. This leads to very slow procedures, as only one gauge volume, one reflection and one orientation is measured at a time. Also, use of the 3DXRD microscope for engineering will often be problematic in that the number of reflecting grains observed by the detector is too few to constitute a valid statistical ensemble.

To overcome such problems we suggest using a conical slit (CS), with openings along the Debye–Scherrer cones of the sample to be investigated. The incoming beam would still be confined by a slit or by focusing, but the detector has to be replaced by a two-dimensional device, such as a CCD camera or an image-plate system. While still probing only one gauge volume at a time, complete information on the texture and strain field can be obtained simultaneously from a set of exposures acquired while rocking the sample around one axis. Also, by averaging azimuthally along the Debye–Scherrer cones, more reflecting grains are observed. Moreover, in general, sample environments can be simplified as, for example, Eulerean cradles are not needed.

This proposal has three main drawbacks. Firstly, one CS will only work for samples belonging to one specific symmetry group and only at one energy. Secondly, aligning the CS is non-trivial; and thirdly, it is difficult to manufacture with high precision.

We have manufactured a CS with six cones, each with a gap of 25 μm, by the wire-electrodischarge machining (wire-EDM) method. The CS is 4 mm thick, made of tungsten carbide, and designed for studies of face-centred cubic (f.c.c.) materials (Al, Ni, Cu . . .) at X-ray energies just above the tungsten *K*-edge. The EDM technique is routinely used in the toolmaking industry for generation of mould inserts or dies for punching purposes (Richter *et al.*, 1997). It offers a high degree of freedom in manufacturing complicated components with a form accuracy of ±1/±2 μm and a surface quality between R_a = 0.1 μm and 0.2 μm (Nienhaus *et al.*, 1998; Wolf *et al.*, 1998) where R_a is the average surface roughness. It also provides a simple solution to the problem of assembling the conical parts.

In this paper we first present the geometric principle and discuss the obtainable depth resolution. Next the specifications for the CS are given and the manufacturing process described. Then we present a strategy for alignment of the device in the X-ray beam and give test results for the machining and assemblage errors. Then we present the results of a feasibility study related to mapping of grain boundaries and grain orientations in a Cu polycrystal. [The main use of the slit is expected to be local strain and stress measurements. First results will be published elsewhere (Withers, 1998; Lienert, Martins *et al.*, 1999).] Finally, we discuss the prospect of the technique in view of the accuracy of manufacturing.

2. Geometric principle

The geometry underlying the principle is illustrated in Fig. 1. A monochromatic beam is defined in two directions either by a pinhole or by focusing. A conical device is mounted behind the sample with a suitable two-dimensional detector positioned further downstream.

The device has conical openings with a constant gap, positioned in accordance with the Debye–Scherrer cones from an ideal powder of the material to be investigated at the chosen X-ray energy. A central hole is added to allow the monochromatic beam to be absorbed in a beam stop of suitable dimensions. This hole is also useful for pre-alignment. Sample translations are denoted (x, y, z) with x along the beam, and scattering angles by 2θ. ω denotes a rotation of the sample around the vertical axis. If focusing is used, the energy bandwidth and divergence has to be correlated to the design of the conical device (gap, divergence of openings, distance to sample).

By varying the material thickness and the gap, the conical device can be designed to work as a slit or as a collimator. As a slit the strain profile can be directly monitored in the images provided the two-dimensional detector has a sufficient resolution. Moreover, for coarse-grained samples the integrated intensity of a reflection from a single grain can be deduced from a single exposure acquired while oscillating the sample in ω. For fine-grained samples, the option of summing over the strain profile implies that texture components are directly observable. As a collimator, only a part of the strain profile is allowed to pass. Hence, neither strains nor integrated intensities are directly observable. Instead it is necessary to scan the incoming energy. Intensities will also be substantially lower in this case.

The depth resolution Δ_x is an issue. For an infinitesimally small incoming beam and an ideal collimator, Δ_x is given by the projection of Δ, the gap of the ring: $\Delta_x = \Delta/\tan(2\theta)$. Hence, with a constant gap the resolution improves with increasing Bragg angles. For a slit, at first thought the resolution will be worse, depending on geometric factors such as the sample-to-slit distance and the divergence of the incoming beam. However, provided the two-dimensional detector has an appropriate spatial resolution and is positioned sufficiently far behind the slit, ray-tracing

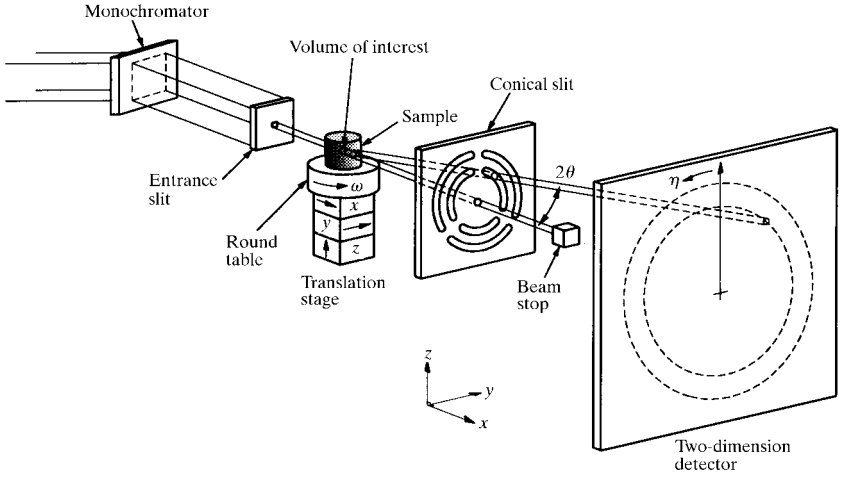

Figure 1
Geometry of the proposed principle. The CS confines the diffracted beam from a specific gauge volume in the sample.

approaches can be applied. The depth resolution can then be maintained at the level of a collimator. A detailed description and proof of such a reconstruction technique for local strain measurements will be given elsewhere (Lienert, Martins *et al.*, 1999).

In this paper we will only be concerned with the slit alternative. In the limit of an infinitesimal thin slit the conical openings will be rings. This is the term we will apply.

3. Design and manufacture

The CS was constructed by wire-EDM, a thermal material removal process based on the action of electrical discharges between a tool electrode and a workpiece. EDM-machining basically allows the machining of all conductive material, disregarding its mechanical properties such as hardness, tensile strength *etc*. Material in the working zone is melted and afterwards removed through a surrounding dielectric liquid. However, neighbouring sections also suffer from the induced heat. Microcracks and material layers with changed properties several micrometres thick are the result. In addition, electrolysis at edges is a known problem, but trim cuts with lowest discharge energy remove the heat-effected layers and provide a smooth surface finish on demand.

The width of the CSs was designed to be 25 μm but wire-EDM is only possible with wires down to diameters of 30 μm. This makes it impossible to manufacture the six CSs in a single piece of tungsten. Instead, seven conical parts were manufactured and assembled afterwards (see Fig. 2).

The conical parts are designed with small uniform tabs (see Fig. 2) to make the cones self-aligning when assembled. The CS is designed to accept the centre beam and six powder reflections, corresponding to the (111), (200), (220), (222), (331) and (422) reflections from an f.c.c. powder. The design of the CS is based on an Ag powder with a lattice constant $a_{\mathrm{Ag}} = 0.40862$ nm, positioned 10 mm in front of the CS, and an X-ray energy of 69.263 keV. Other f.c.c. materials can be investigated by changing the energy. The thickness of the device is 4 mm. Hence, the intrinsic divergence is 6×10^{-4}, which is sufficient that it works as a slit for undeformed or lightly deformed materials.

For the fabrication of the cones a tungsten wire with a diameter of 0.1 mm was used. The EDM-machining was performed using an AGIECUT 150 HSS+F, which has a maximum taper angle of $\pm 15^{\circ}$.

The following procedure was applied. In the first step a tungsten carbide block was precisely ground. Then starting holes for wire-EDM were structured by EDM-die sinking using rotating cylindrical electrodes. With these prerequisites the generation of the inner structures could be performed by wire-EDM. Immediately, in the same fabrication step, the outer structure with the tabs was also machined by wire-EDM. This procedure guaranteed the exact concentricity between the inner and the outer structure of each individual part. However, it was found that slightly misaligned wire electrodes resulted in elliptically shaped cones instead of cones with a circular cross section. Following this fabrication procedure, misalignment errors tend to build up between the outermost and the innermost ring. For this reason the cones put into the CS were carefully measured, selected and assembled.

4. Alignment

In this section we address the problem of aligning the CS with respect to the monochromatic beam. This task is non-trivial owing to the six degrees of freedom involved: the wavelength of the incident radiation and the three translations and two tilts of the CS. Also, the requirements for precision are high: a few micrometres tolerance on the position and 0.5 mrad on the tilts. We will assume that the machining and assembly errors are negligibly small. A perfect alignment is then obtained if, and only if, the intensity distribution of all the rings in the image are isotropic.

We suggest an alignment procedure where the incoming beam is defined (by slits or focusing) to a spot with dimensions substantially smaller than the gap of the CS. A thin foil should serve as a test sample, with the surface normal placed parallel to the incoming beam. The thickness should be small compared with the expected depth resolution. The foil may be amorphous or a fine-grained well-annealed f.c.c. powder with a random texture.

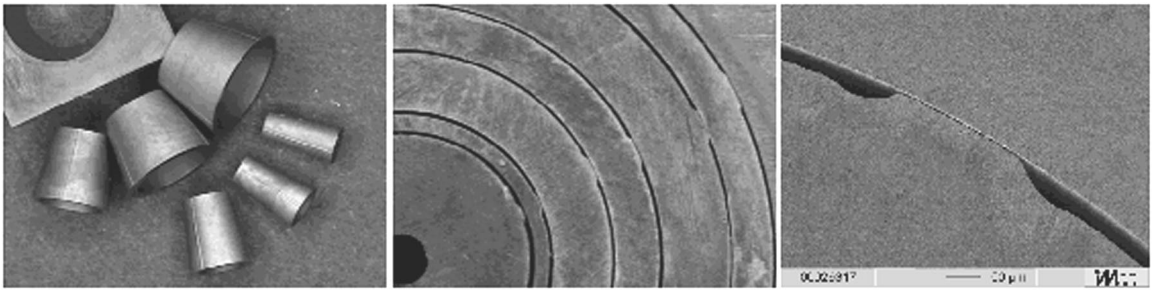

Figure 2
Left: the seven conical parts of the CS. Middle: top view of the assembled system. Right: one tab between two parts providing a constant slit width of 25 μm.

In the following we present a formula for the misalignment of one ring. Based on this we discuss a strategy for the alignment of the CS.

4.1. *Formalism*

The geometry of one Debye–Scherrer cone and the corresponding ring of the CS is illustrated in Fig. 3. The coordinates of the centre of the ring are (x_c, y_c, z_c), while tilts around the y- and z-axes are denoted ω_c and χ_c, respectively. 2Θ is the opening angle of the slit and η is defined as the azimuthal angle in the images, with $\eta = 0$ at the 12 o'clock position. $\Delta 2\theta$ is an angular offset caused by an energy perturbation. The diffraction volume is situated at $(-L, 0, 0)$.

As seen from Fig. 3, a misalignment of the ring is related to an angular offset $\delta 2\Theta$ between the ring and the Debye–Scherrer cone. The aim of the alignment is to bring $\delta 2\Theta$ to zero for all angles η. Then $x_c = y_c = z_c = \chi_c = \omega_c = \Delta 2\theta = 0$. With these definitions the following equation applies, provided the ring is pre-aligned within a few degrees,

$$\begin{aligned}\delta 2\Theta = & -\left[\Delta 2\Theta + (x_c/2L)\sin 4\Theta\right] \\ & -\cos^2 2\Theta\left\{\sin\eta\left[(y_c/L) + \omega_c \tan^2 2\Theta\right]\right. \\ & \left.+\cos\eta\left[-(z_c/L) + \chi_c \tan^2 2\Theta\right]\right\}. \qquad (1)\end{aligned}$$

Each bracket of this equation contains pairs of position and angular parameters which are 'coupled' as they can compensate each other. Note that for the CS as a whole the compensation only works for one ring at a time, due to the difference in 2Θ values.

4.2. *Alignment strategy*

The intensity transmitted through one ring of the CS and observed on the two-dimensional detector has an appearance which reflects the misalignment. Typical intensity patterns are presented in Fig. 4. Analysing the geometry of the patterns and applying equation (1), the CS can be aligned in numerous ways. We outline one algorithm, comprising three steps.

Step 1. The second term in the equation changes sign when substituting η with $\eta + 180°$. Acquiring images while scanning the CS along the x-axis, intensities will therefore peak simultaneously at opposite positions if, and only if, the first term is zero. By performing such a scan and identifying positions of maximum intensity for η and $\eta + 180°$ in several rings, then equation (1) can be solved for $\Delta 2\theta$ and x_c.

Step 2. With the first term in the equation being zero, we focus on one ring (one 2θ value). In general, the situation will be as illustrated in Fig. 4(b), with two peaks centred at η with $\eta + 180°$. A combined y_c and z_c scan along a line perpendicular to the line connecting the two spots is performed. The (y_c, z_c) positions are noted, where isotropic illumination of the ring is obtained. The CS is now aligned with exception of the redundancy between y_c and ω_c and between z_c and χ_c.

Step 3. Step 2 is repeated for the other rings. Based on equation (1), a global least-square optimization of y_c, z_c, ω_c and χ_c is extracted from the set of optimal $[y_c(2\theta), z_c(2\theta)]$ positions.

5. Test of the CS

The seven parts shown in Fig. 2 were mounted individually into a scanning electron microscope. From the micrographs it was found that the main machining error relates to the eccentricity of the cones. To quantify this error, the inner and outer diameters were determined in two directions (up/down and left/right) and on both sides (front/back) of each piece. The resulting absolute error on the diameter is at worst 13 µm and on average 4.6 µm.

Following assembly, a full test of the perfection of the CS was performed at the synchrotron beamline ID15, ESRF. The test sample was a 100 µm-thick layer of an Ni reference

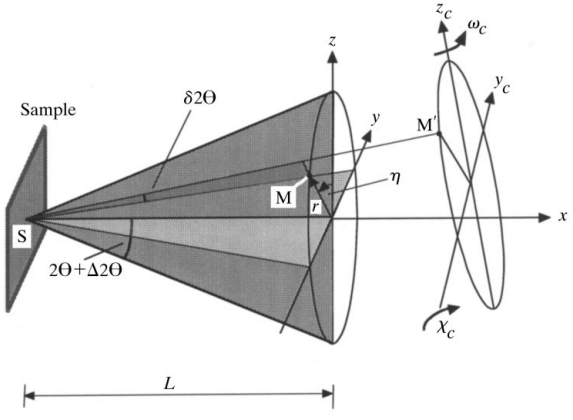

Figure 3
Geometry related to CS movements. Illustration of one Debye–Scherrer cone and a misaligned slit. The Debye–Scherrer cone is diffracted by a thin powder sample illuminated with a narrow beam. The direct beam is along the x-axis. For a given angle η the misaligned ring in the CS selects the direction SM′ instead of the beam direction SM leading to an angular offset of $\delta 2\Theta$ with respect to the Debye–Scherrer cone.

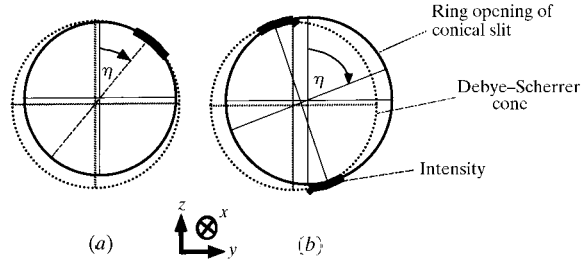

Figure 4
Typical intensity distributions on a two-dimensional X-ray detector behind the CS for a misalignment between the CS and the Debye–Scherrer cone. (a) The CS is not aligned along x. Projected onto the X-ray detector, the ring of the CS is smaller than the Debye–Scherrer cone. Only for a small range around the angle η is the Debye–Scherrer cone seen on the screen. (b) The CS is aligned along x. Parts of the Debye–Scherrer cone are seen at the angles η and $\eta + 180°$ due to a misalignment of the orientation and the transversal position (y_c and z_c) of the CS.

powder, packed between two glass plates. As described by Suortti (1977), the reference powder is well annealed and has virtually no strain. The experiment took place at the 'port hutch' experimental station, where two-dimensional focusing cannot be provided. Instead, the incoming beam was defined by a square aperture to 22 μm × 24 μm. The beam profile was found to be almost Gaussian in both directions. The two-dimensional detector was an image intensifier placed 30 cm from the test sample.

The CS was aligned with respect to the (200) ring by the procedure outlined in §4. A resulting short time exposure is shown in Fig. 5.

The CS was translated in x, y and z within a three-dimensional mesh. At each position an exposure was made. For each exposure and each ring the azimuthal variation of intensity was evaluated using *FIT2D* (Hammersley *et al.*, 1996). Based on this information the global assembly error of the seven parts can be estimated by comparing the 'focal point' of the rings, *i.e.* the (x, y, z) settings where the individual rings are aligned (the optimal isotropy). Moreover, the spatial resolution can be determined from the widths of the intensity distributions during scanning.

As an example of the results, we report on the depth resolution obtained for the various reflections. The analysis was based on an x-scan through the (200) alignment centre. Thirteen images were recorded at equidistant positions within a total range of 1300 μm. For each ring the intensity was integrated radially as well as azimuthally, omitting the areas that correspond to the beam stop. Next, the variation of the integrated intensity with x was fitted to a Gaussian. The resulting fitted midpoints and widths are listed in Table 1. The table also contains calculated values for the widths, assuming the machining and assemblage errors to be absent. The two outermost rings are not included, owing to a lack of recorded intensity.

From Table 1 the measured and calculated depth resolution is seen to be in reasonable agreement, with better resolution for higher-order reflections as expected. The combined effect of the assembly and aligning errors makes the slits look more narrow seen from the diffracted beam and that causes the measured depth resolution to be smaller then the calculated value. The midpoints are constant within measurement error, with the exception of the (111) reflection, which is offset by 150 μm. The magnitude of this offset, seen in relation to the measured width, implies that assembly errors have caused the focal point of the (111) reflection to be shifted. In general, we estimate the average machining and assemblage errors on the diameter of the CS rings to be both of the order of 5 μm.

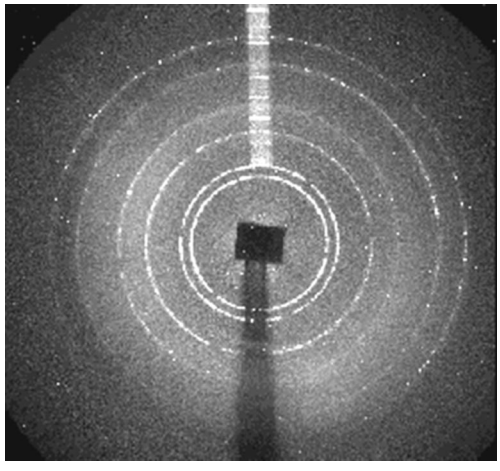

Figure 5
A typical powder test pattern.

Table 1
The calculated and measured depth resolution for the four innermost rings in the CS.

Experimental results are based on Gaussian fits to the variation of the total intensity (summed over η; *cf.* Fig. 3) with translation along the beam. Also included are the fitted centre positions, with arbitrary zero-point.

Reflection	Calculated FWHM (μm)	Measured FWHM (μm)	Measured centre position (μm)
(111)	366	275 ± 12	654 ± 5
(200)	315	222 ± 12	807 ± 6
(220)	239	217 ± 16	817 ± 7
(222)	181	192 ± 15	811 ± 7

6. Application: grain boundary mapping

As an example of application we summarize the results of a feasibility test performed at beamline ID11, ESRF. The aim was to map grain boundaries and grain orientations within embedded layers of a coarse-grained 4.5 × 4.5 × 4.5 mm-sized Cu polycrystal. Following sectioning of the sample, the results were then compared with electron microscopy (EBSP) data on the same layers.

The set-up was identical to the one presented in Fig. 1, with the incoming beam being defined by a 50 μm × 50 μm aperture. Results shown here refer to one specific layer and the (200) data only. To find the orientation of a specific grain the sample was first rotated from −90° to 90° in steps of 10° while oscillating by ±5° at each step. By identifying at least three major spots relating to lattice planes that are perpendicular to each other, a first fit is obtained. Next, the exact orientation is determined by acquiring exposures at constant ω and 'scanning' ω with an accuracy of $\Delta\omega = 0.1°$. To map a specific grain the variation in total intensity of a selected reflection is monitored while scanning the gauge volume in x and y. The boundary is defined to be at the half-intensity point, and is found by interpolation.

Resulting synchrotron and EBSP data are shown in Fig. 6. The map provided by synchrotron diffraction is not complete owing to an inadequate amount of beam time (of the order of 12 h). Grain positions measured by the two methods correspond within 150 μm and orientations within 2°.

There is a large potential for substantial improvements of these numbers, especially the spatial accuracy. Firstly, the

impinging beam size can be reduced to 5 μm × 5 μm by focusing, as discussed above. Secondly, measuring several reflections from the same grain, corresponding to approximately 90° sample rotations, can diminish the effect of the poor resolution in the direction along the beam. Thirdly, slight misalignments during synchrotron measurement implied that the measured layer is not identical to the surface measured by EBSP.

7. Discussion

Häuserman & Itié (1992) have previously reported the use of a conical device in the diffracted beam. In their case the device was a conical collimator with one ring used for 'beam cleaning' and energy determination in high-pressure research. To our knowledge the present work is the first attempt to use such a device for depth profiling or three-dimensional mapping in X-ray diffraction. In this respect we note that the device might in fact be even more useful for energy-dispersive work, in connection with energy-sensitive two-dimensional detectors. However, at present such detectors (annular rings of solid-state detectors) have a very limited spatial resolution. The basic principle can naturally be applied to X-rays with lower energies or to neutrons, but in these cases flat conical devices and flat two-dimensional detectors cannot be used due to the larger scattering angles.

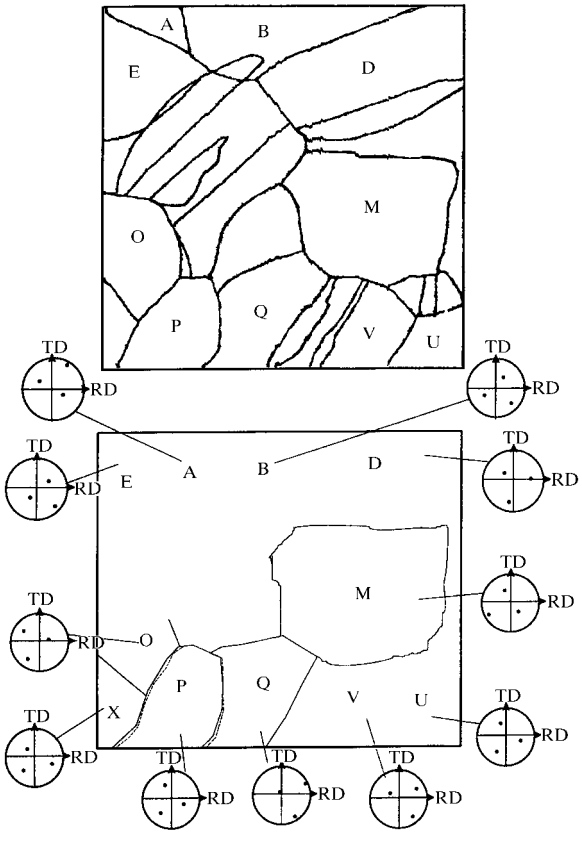

Figure 6
Grain mapping of the top layer in a Cu polycrystal by electron microscopy (EBSP) (top), and using the hard X-ray CS set-up illustrated in Fig. 1 (bottom). Also shown are the determined ⟨200⟩ pole figures for the individual grains. The boundary of grain P was measured using a (200) reflection from grain P (solid line) as well as (200) reflections from neighbouring grains X, O and Q (dashed lines).

The CS described in this paper is designed for f.c.c. materials and a particular energy, which limits the applicability. The conical parts all suffer from some degree of eccentricity, even though the most modern wire-EDM machining was used to produce the conical parts. When assembled, the achieved slit width is approximately 25 ± 5 μm. This uncertainty influences the resolutions of the CS and makes it difficult to compare intensities through different rings.

The assembly errors could have been avoided if it had been possible to manufacture the six slits in one piece of tungsten. When the slit is assembled from seven conical pieces the combined machining and assembly errors could be determined by performing a calibration of the CS. The procedure outlined in §5 would be suitable for that. However, this would complicate the data analysis substantially.

The tab system that ensures the self-alignment of the cones needs to be modified. Structuring the inside of the cones and at the same time increasing the height of tabs (*e.g.* to 75 μm) on the outside would definitely lead to an improvement. Alignment and tilting errors between the cones due to the geometrical errors of tabs over the entire height could be minimized. The cones would be secured against each other. Therefore, distortion could be excluded as well. A better self-aligning system for the cones in the CS would ensure that all slit openings focus on the same gauge volume, and cross-eyed slits like the (111) ring would be avoided.

A straightforward way of reducing the errors is to make the conical device thinner. This is feasible, as the penetration depth at 70 keV is 62 μm. Hence, even at a thickness of 1 mm the transmitted fraction is 10^{-7}. A thinner device would also constitute a more ideal slit. On the other hand, conical collimators of, *e.g.* 30 mm thickness, are available with the technology presented here.

8. Conclusions

A novel diffraction technique has been presented. The potential will depend on the machining and assembly accuracy of the conical device. With errors as obtained here (5–10 μm) the main applications are foreseen to be within materials engineering – local stress and local texture determinations. Suggestions for improving the manufacturing process are given, sustaining ambitions of also using the technique within physical metallurgy.

This work was sponsored by the Danish National Research Councils through the Engineering Science Centre

for 'Structural Characterization and Modelling of Materials' at Risø and through Dansync. The authors would like to thank C. Klitholm for design of the translation stage, and V. Honkimäki for help during synchrotron experiments. Fruitful discussions with D. Juul Jensen and E. Johnson are acknowledged. In addition, we are grateful for the general support at beamlines ID11 and ID15, ESRF, to this project.

References

Hammersley, A. P., Svensson, S. O., Hanfland, M., Fitch, A. N. & Häusermann, D. (1996). *High Press. Res.* **14**, 235–248.

Häuserman, D. & Itié, J. P. (1992). *Rev. Sci. Instrum.* **63**(1), 1080–1082.

Lienert, U., Martins, R., Grigull, S., Pinkerton, M., Poulsen, H. F. & Kvick, Å. (1999). *Proceedings of the MRS99 Fall Meeting: Applications of Synchrotron Radiation Techniques to Materials Science.* In the press.

Lienert, U., Poulsen, H. F. & Kvick, Å. (1999). *Proceedings of the 40th AIAA Structures, Structural Dynamics and Materials Conference*, pp. 2067–2075, St Louis, MO, USA.

Lienert, U., Schulze, C., Honkimäki, V., Tschentscher, T., Garbe, S., Hignette, O., Horsewell, A., Lingham, M., Poulsen, H. F., Thomsen, N. B. & Ziegler, E. (1998). *J. Synchrotron Rad.* **5**, 226–231.

Nienhaus, M., Ehrfeld, W., Michel, F., Graeff, V. & Wolf, A. (1998). *Proc. Micromach. Microfabr. Process Technol. IV*, **3511**-13, 135–142.

Poulsen, H. F., Garbe, S., Lorentzen, T., Juul Jensen, D., Poulsen, F. W., Andersen, N. H., Frello, T., Feidenhans'l, R. & Graafsma, H. (1997). *J. Synchrotron Rad.* **4**, 147–155.

Richter, T., Ehrfeld, W., Wolf, A., Gruber, H. P. & Wörz, O. (1997). *Proceedings of the First International Conference on Microreaction Technology*, pp. 158–168. Berlin: Springer Verlag.

Suortti, P. (1977). *Acta Cryst.* A**33**, 1012–1027.

Withers, P. J. (1998). Personal communication.

Wolf, A., Ehrfeld, W., Michel, F., Koch, O., Preuß, S., Soultan, H. & Gruber, H. P. (1998). *Proc. SPIE*, **3517**, 149–158